

All-electron quasi-particle self-consistent GW band structures for SrTiO_3 including lattice polarization corrections in different phases

Churna Bhandari

Department of Physics and Astronomy, University of Missouri, Columbia Missouri

Mark van Schilgaarde

Department of Physics, King's College London, London WC2R 2LS, United Kingdom

Takao Kotani

Department of Applied Mathematics and Physics, Tottori University, Tottori 680-8552, Japan

Walter R. L. Lambrecht

Department of Physics, Case Western Reserve University, Cleveland, OH 44106-7079

The electronic band structure of SrTiO_3 is investigated in the all-electron QSGW approximation. Unlike previous pseudopotential based QSGW or single-shot G_0W_0 calculations, the gap is found to be significantly overestimated compared to experiment. After putting in a correction for the underestimate of the screening by the random phase approximation in terms of a 0.8Σ approach, the gap is still overestimated. The 0.8Σ approach is discussed and justified in terms of various recent literature results including electron-hole corrections. Adding a lattice polarization correction (LPC) in the $\mathbf{q} \rightarrow 0$ limit for the screening of W , agreement with experiment is recovered. The LPC is alternatively estimated using a polaron model. We apply our approach to the cubic and tetragonal phases as well as a hypothetical layered post-perovskite structure and find that the LDA (local density approximation) to GW gap correction is almost independent of structure.

I. INTRODUCTION

It is well known that the density functional theory in its commonly used local density and generalized gradient approximations (LDA and GGA) does not provide accurate electronic band structures and in particular underestimates band gaps. This is by now recognized to be mostly because the Kohn-Sham eigenvalues in this theory should not be interpreted as one-electron excitations. To calculate the latter, a many-body-perturbation theory, including a dynamical self-energy, such as the GW approximation, provide a much better justified and more accurate framework. For standard tetrahedral semiconductors, the GW method has been shown to provide accurate gaps. Still, this depends on details of the implementation, for example, all-electron results may differ from pseudopotential results and the level of self-consistency used in the GW method and its convergence versus various parameters plays a significant role. For transition metal and complex oxides, it is still far less clear how well the GW method performs. Here we consider SrTiO_3 as a case study.

We use the all-electron full-potential linearized muffin-tin orbital (FP-LMTO) implementation^{1,2} of the quasi-particle self-consistent (QS) GW method^{3,4} and compare its results for SrTiO_3 with previous results in literature.⁵⁻⁸

II. LITERATURE REVIEW

Sponza *et al.* performed G_0W_0 calculations of the band structure starting from a pseudopotential LDA calculation including Sr $4s, 4p$ and Ti $3s, 3p$ semicore states as valence. They obtain the vertical gap at Γ to be 3.76 eV in good agreement with experiment, whereas their LDA calculation gave 2.21 eV. The actual valence band maximum (VBM) at R is slightly higher than at Γ resulting in a smaller indirect gap both in LDA and in GW . The focus of their paper is on the optical dielectric function including electron-hole interaction effects.

Hamann and Vanderbilt (HV)⁶ performed QSGW calculations using maximally localized Wannier functions (MLWF) to interpolate the self-energy Σ matrix between \mathbf{k} mesh-points on which the QSGW is performed. A similar functions is played by the atom centered muffin-tin-orbitals in our approach. They include only Sr- $4p$ semicore states as valence electrons. Both these groups used the ABINIT package but used somewhat different cut-off parameters. Their plane-wave cut-off for the basis set is similar but HV used a smaller number of unoccupied bands. They obtained the indirect LDA gap of 1.61 eV and a GW gap of 3.32 eV. Curiously, the gap correction of HV (1.71 eV) is larger than that of Sponza *et al.* (1.55 eV). They did not mention the direct gap at Γ , but assuming all LDA calculations considered here get similar value for this difference, we'll use our LDA value (0.44 eV) for the difference between the VBM at R and Γ . HV's direct gaps at Γ would then amount to 2.05 eV (LDA) and 3.76 eV (GW). Thus, these two pseudopotential calculations are in good agreement with each other in spite of the

small changes in parameter choices. The main point of HV's paper is that the MLWF interpolation works well and indicates little change in the Wannier functions extracted from LDA or GW calculations.

A third pseudopotential based *GW* calculation by Cappellini *et al.*⁷ obtained significantly different results. They also include Sr 4*s*, 4*p*, Ti 3*s*, 3*p* as valence electrons and obtain an LDA gap at Γ of 2.24 eV (indirect $R-\Gamma$ of 1.90) but *GW* gaps of 5.42 eV ($\Gamma-\Gamma$) and 5.07 eV ($R-\Gamma$). The reason for this discrepancy is unclear but presumably is related to the use of a model dielectric function instead of a consistently calculated one. Finally, a previous FP-LMTO QSGW calculation by Kotani *et al.*,^{8,9} gives the indirect gap at Γ of about 4.25 eV but gave few details.

From the above, it appears from the pseudopotential calculations that the G_0W_0 gap is close to that of the QSGW gap, and that both are in good agreement with experiment. The all-electron QSGW gap however seems to be about 1 eV larger than experiment. Here we further investigate this issue.

III. METHODS

The QSGW approximation as implemented in FP-LMTO was described in detail in Ref. 4. The idea behind the QSGW method is to make an optimal choice of the H_0 Hamiltonian so that its Kohn-Sham eigenvalues ϵ_i are as close as possible to the quasiparticle energies E_i . To do this, a hermitian but non-local exchange correlation potential, specified by its matrix in the basis of the H_0 eigenstates,

$$[V_{xc}^{\Sigma}]_{ij} = \frac{1}{2} \text{Re}[\Sigma_{ij}(E_i) + \Sigma_{ij}(E_j)], \quad (1)$$

is used in H_0 . Here, $\Sigma(\omega)$ is the energy dependent self-energy calculated from $G_0(\omega)$, the one-electron Green's function corresponding to H_0 , in the single-shot *GW* approximation: $\Sigma = iG_0W_0$. Starting from an LDA H_0 , Σ is calculated, $V_{xc}^{\Sigma} - V_{xc}^{LDA}$ is added to H_0 , a new G_0 calculated and so on till self-consistency. The reasons behind this approach and differences from fully self-consistent *scGW* are discussed in Refs. 4, 8, and 10.

For tetrahedral semiconductors, this approach provides systematically a $\sim 20\%$ overestimate of the gap due to the underestimate of the dielectric screening in the random phase approximation (RPA) which does not include electron-hole effects and thus misses ladder diagrams in the evaluation of the irreducible polarization propagator $\Pi^0 = -iG_0 \times G_0$, which determines W through $W = (1 - v\Pi^0)^{-1}v$, where v is the bare Coulomb interaction and a simplified symbolic operator notation is used. This has led to the adoption of a universal 0.8Σ correction factor.^{9,14,15} This is illustrated in Fig. 1 which shows the typical underestimate of screening by QSGW to be 20% as indicated by the dashed line. Although it is not clear *a priori* that this also applies to oxides we adopt a similar correction factor here.

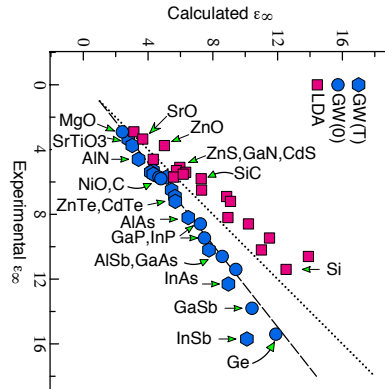


FIG. 1. QSGW (blue) and LDA (red) optical dielectric constant ϵ_{∞} compared to experiment. Experimental data for GW(T) is taken at room temperature; for GW(O) 0K data is used. LDA data for NiO is not shown because it is off the scale; similarly the narrow gap semiconductors InAs, GaSb, InSb and Ge where the LDA gap is negative. The dotted line would indicate perfect agreement between calculation and experiment, while the dashed line corresponds to 20% underestimate by the calculation.

It is interesting that ϵ_{∞} predicted by the LDA is in sometimes better agreement with experiment. This can be attributed to a fortuitous cancellation of errors: missing ladder diagrams tend to cause ϵ_{∞} to be underestimated, while the LDA's gap underestimate contributes an error of the opposite sign. There is no universal pattern, however, as is already apparent in the data shown in Fig. 1. Where gap errors are severe the LDA severely overestimates the ϵ_{∞} . For example in NiO, the $\epsilon_{\infty}^{LDA} > 30$.

Further justification for the 0.8Σ correction factor can be obtained from the work of Shishkin, Marsman and Kresse (SMK)¹³ and Wei and Pasquarello (WP),¹¹ who added an exchange-correlation kernel to the screening of the polarization function $\tilde{\Pi} = [1 - (v + f_{xc})\Pi^0]^{-1}$ using the nanoquanta kernel or a bootstrap kernel respectively. We will refer to their approach as QSG \tilde{W} . Although these kernels primarily address the $\mathbf{q} \rightarrow 0$ and static ($\omega = 0$) behavior and might thus not capture the full extent of the electron-hole effects on renormalizing the screening in W , and have received some critical discussions,¹⁶ it is useful in the present context to analyze how much they affect the gaps for a variety of materials. Analyzing the data in Table I in WP, part of which is reproduced here in Table I with additional analysis, we find that $[E_g(\text{QSG}\tilde{W}) - E_g(\text{LDA})] / [E_g(\text{QSGW}) - E_g(\text{LDA})]$ has an average value of about 0.76 with standard deviation of 0.04 with the largest deviation for NiO, where it is 0.85 and ZnO, 0.68. ZnO, is a notably difficult material to converge and SMK's values for the QSGW and QSG \tilde{W} gaps would give 0.77. NiO is a well-known strongly corre-

TABLE I. LDA, QSGW and QSG \tilde{W} gaps, gap corrections and their ratios from Ref. 11, scGW+vertex from Ref. 12. B and D refer to two different vertex correction schemes, see text.

	E_g			ΔE_g		Ratio	E_g			ΔE_g			Ratio	
	LDA	QSGW	QSG \tilde{W}	QSGW-LDA	QSG \tilde{W} -LDA	$\frac{\Delta E_g^{\text{QSG}\tilde{W}}}{\Delta E_g^{\text{QSGW}}}$	scGW	B	D	scGW-LDA	B-LDA	D-LDA	B	D
MgO	4.65	9.29	8.30	4.64	3.65	0.79	9.31	8.24	7.96	4.66	3.59	3.31	0.77	0.71
NiO	1.05	4.97	4.40	3.92	3.35	0.85								
TiO ₂	1.90	4.22	3.73	2.32	1.83	0.79								
Cu ₂ O	0.53	2.65	2.12	2.12	1.59	0.75								
ZnO	0.85	4.61	3.42	3.76	2.57	0.68								
C	4.22	6.4	5.9	2.18	1.68	0.77	6.15	5.8	5.73	1.93	1.58	1.51	0.82	0.78
SiC	1.39	2.9	2.52	1.51	1.13	0.77	2.89	2.52	2.42	1.50	1.13	1.03	0.75	0.69
GaAs	0.43	1.75	1.51	1.32	1.08	0.75	2.27	1.80	1.72	1.84	1.37	1.29	0.74	0.70
BN	4.53	7.51	6.67	2.98	2.14	0.74								
LiCl	6.52	10.98	9.87	4.46	3.35	0.74								
Si	0.57	1.47	1.3	0.9	0.73	0.76	1.55	1.32	1.26	0.98	0.75	0.69	0.77	0.70
LiF ^a	9.28	15.90	14.50	6.62	5.22	0.79	16.3	15.02	14.39	7.02	5.74	5.11	0.82	0.73
Ge	0.00	0.96	0.82	0.96	0.82	0.76								
AlP	1.60	3.1	2.77	1.5	1.17	0.75	2.84	2.53	2.44	1.24	0.93	0.84	0.75	0.68
CdS	1.21	3.41	2.74	2.2	1.53	0.75								
Average						0.76							0.78	0.72
Stdv						0.04							0.04	0.04

^a From SMK¹³

lated material and a deviation here is not too unexpected. We note that multiplying the self-energy operator Σ by 0.8 is not exactly the same as correcting the gap shift by 0.8. A slightly larger gap reduction typically occurs.

Very recently, Kutepov^{12,17} introduced a way to solve Hedin's full set of equations^{18,19} beyond the GW approximation using systematic diagrammatic approximations for the vertex function. First of all, his results show fully self-consistent sc GW results differ only slightly from the QSGW results and tend to overestimate the band gaps by a similar amount. Secondly, he used two different self-consistency schemes which both introduce vertex corrections both in G and Π . The results of his scheme B, which in his notation only includes a first correction to the vertex Γ_1 , are close to those of SMK and WP where comparison for the same material is possible (Si, LiF, GaAs, SiC, BN, MgO) while his most advanced scheme including the full Γ_{GW} vertex, give a somewhat larger reduction of the gap. These are also shown in Table I. Viewed as percentage of the sc GW -GGA (or LDA) correction they give correction factors of about 0.78 and 0.72 respectively when averaged over various cases. As an example for MgO, his sc GW gap is 9.31 and his schemes B and D give 8.24, 7.96 eV while WP's QSGW and QSG \tilde{W} give 9.29, 8.30 eV and SMK obtain 9.16 eV, 8.12 eV respectively. The scheme D agrees almost perfectly with experiment when a lattice-polarization correction of 0.15 eV added to the experimental volume but the latter may be somewhat underestimated.²⁰ In any case, these

results also support that the electron-hole correction effects beyond RPA amount to about a 20 % reduction of the QSGW gap correction beyond LDA or GGA.

Besides the electron-hole corrections discussed until now, we also consider a lattice-polarization correction as suggested by Botti and Marques (BM)²¹ and revisited recently in Ref. 20. The idea here is that for strongly ionic materials, with large LO-TO phonon splittings, the W in the long-wave length limit $W(\mathbf{q} \rightarrow 0, \omega)$ should include the effects of the ionic displacements on the macroscopic dielectric constant. The macroscopic dielectric constant enters the calculation of Σ in the special treatment of the $\mathbf{q} \rightarrow 0$ region in the convolution integral over \mathbf{k} -space:

$$\Sigma_{nm}^c(\mathbf{k}, \omega) = \frac{i}{2\pi} \int d\omega' \sum_{\mathbf{q}} \sum_{n'}^{BZ \text{ all}} G_{n'n'}(\mathbf{k} - \mathbf{q}, \omega - \omega') \sum_{\mu\nu} W_{\mu\nu}^c(\mathbf{q}, \omega') e^{-i\delta\omega'} \langle \psi_{\mathbf{k}n} | \psi_{\mathbf{k}-\mathbf{q}n'} E_{\mu}^{\mathbf{q}} \rangle \langle E_{\nu}^{\mathbf{q}} \psi_{\mathbf{k}-\mathbf{q}n'} | \psi_{\mathbf{k}m} \rangle \quad (2)$$

Here, a two-particle mixed product interstitial-plane-wave basis set E_{ν} diagonalizing the bare Coulomb interaction matrix is used^{4,22} and W^c is the correlation part of W , subtracting the bare exchange. The need for a special treatment of the $\mathbf{q} \rightarrow 0$ region arises from the integrable divergence of the Coulomb interaction ($\propto 1/q^2$) and is here treated using the modified offset- Γ method,²³ which in turn is closely related to the analytic $\mathbf{k} \cdot \mathbf{p}$ scheme of Friedrich *et al.*²² This involves the macroscopic dielectric

tensor $\mathbf{L}(\omega)$, in their notation $\mathbf{e}_{\mathbf{k}}^T \mathbf{L}(\omega) \mathbf{e}_{\mathbf{k}}$. The projection along unit vectors $\mathbf{e}_{\mathbf{k}}$ takes care of the non-analytic (orientation dependent) nature of the $\mathbf{k} \rightarrow 0$ limit and fully takes into account any possible anisotropies depending on the crystal structure. It is this macroscopic dielectric tensor, usually written $\epsilon(\omega)$ which needs to be modified to take into account the lattice polarization effect. This is most easily done by means of a Lyddane-Sachs-Teller factor:

$$\frac{\epsilon_{tot}^{\alpha}(\mathbf{q} \rightarrow 0, \omega)}{\epsilon_{el}^{\alpha}(\mathbf{q} \rightarrow 0, \omega)} = \prod_m \frac{(\omega_{LOm}^{\alpha})^2 - \omega^2}{(\omega_{TOM})^2 - (\omega + i0)^2}. \quad (3)$$

where the superscript α denotes a projection direction of the tensor, ($\epsilon^{\alpha} = \mathbf{e}_{\alpha}^T \epsilon \mathbf{e}_{\alpha}$). It is clear from this expression that the correction goes to zero for $\omega \gg \omega_L$. In practice we only include it for $\omega = 0$ to avoid the necessity for a careful integration mesh right near the phonon frequency poles. As discussed in Ref. 20 the BM approach gives the long-range or Fröhlich contribution to the Fan-part of the zero-point motion electron-phonon correction of the gap. The \mathbf{q} -point integration mesh that needs to be used is a subtle issue discussed in Lambrecht *et al.*²⁰. The strength of this contribution, applied only at $\mathbf{q} = 0$ for convenience, can be estimated from the polaron length scale, $a_P = \sqrt{\hbar/2m_*\omega_L}$ with m_* the band-edge effective mass and ω_L the relevant LO-phonon frequency. We will discuss later how to apply this in the present case with multiple phonons and a degenerate VBM not occurring at Γ . The polaronic point of view allows us to make an independent estimate of the corresponding gap reduction.

IV. COMPUTATIONAL DETAILS

We employ a generalized FP-LMTO method^{1,2} as implemented in the Questaal package.²⁴ The basis set is specified by two sets of parameters, the smoothing radii R_{sm} and decay lengths (κ) of smoothed Hankel function envelope functions.²⁵ For SrTiO₃ we include (*spdf*, *spd*) for Sr, (*spd*, *spd*) for Ti and (*spd*, *sp*) for O atoms respectively. These indicate the angular momenta included for each κ . The envelope functions are augmented inside the spheres in terms of solutions of the Schrödinger equation and their energy derivative up to an augmentation cut-off of $l_{max} = 4$. In addition, calculations are made with and without the $4p$ ($3p$) local orbitals inside the spheres for Sr and (Ti).

The Brillouin zone integration \mathbf{k} -point convergence and other convergence parameters of the method were carefully tested for cubic SrTiO₃ and similar criteria were adopted for the tetragonal and orthorhombic phases. We also tested result with a larger \mathbf{k} -point mesh and found the band gap is converged within 0.05 eV. Specifically, we used a $4 \times 4 \times 4$ un-shifted mesh for the Brillouin zone sampling, along with the tetrahedron method for the cubic cases in the LDA self-consistent charge convergence and for the calculation of the Σ in *GW*. For the tetragonal phase, the unit cell is larger along the c -direction

TABLE II. Experimental lattice constants (except for orthorhombic structure) in Å and Wyckoff position of atoms SrTiO₃ in various structures for cubic and tetragonal ($c/a = 1.414$ and $w=0.241$).

Symmetry	Lattice constant	Wyckoff position
		Sr(0,0,0) \Rightarrow 1a
Cubic	a=3.905 ^a	Ti(0.5,0.5,0.5) \Rightarrow 1b
		O(0.5,0.5,0.0) \Rightarrow 3c
		Sr(0,0.5,0.25) \Rightarrow 4b
Tetragonal AFD	a=5.507 ^b , c=7.796	Ti(0,0,0) \Rightarrow 4c
		O(0,0,0.25) \Rightarrow 4a
		(w,0.5+w,0) \Rightarrow 8h
Orthorhombic post-perovskite	a=3.01 b= 12.77 c= 5.87	Sr(0,0.2906,0.25) \Rightarrow 4c
		Ti(0,0,0) \Rightarrow 4a
		CaIrO ₃
		O(0,0.4939,0.25) \Rightarrow 4c
		O(0,0.1391,0.999) \Rightarrow 8f

^a Expt. A. Yu. Abramov and *et al.*²⁸

^b Expt. by W. Jauch and *et al.*²⁹

than in-plane by a factor $\sqrt{2}$. Thus, we use accordingly smaller number of \mathbf{k} -points, $4 \times 4 \times 3$ for both LDA and QSGW calculations.

For the self-consistency cycle, the charge density and the total energy are converged within the tolerance of $10^{-5} e/a_0^3$ and 10^{-5} Ry respectively. For QSGW, after several convergence test calculations, we settled the cut-off above which the self-energy matrix is approximated by an average diagonal value, $\Sigma_{cut} = 3$ Ry, including self-energy calculations up to 3.5 Ryd, the interstitial plane wave cut-off energy for basis functions $E_{cut}(\psi_G) = 2.6$ Ry and for the auxiliary basis $E_{cut}(\psi_{coul}) = 2.8$ Ry respectively. In QSGW, the self-consistent iteration was carried until the change in Σ was less than 10^{-4} Ry.

V. CRYSTAL STRUCTURES

We consider the cubic and tetragonal anti-ferroelectrically distorted (AFD) $I4/mcm$ structure occurring at low temperature. In addition we consider the layered orthorhombic CaIrO₃ structure, suggested to occur at high pressures by Cabaret *et al.*²⁶ and also known as the post-perovskite structure. Although we will show elsewhere²⁷ that this structure is unlikely to occur because it has a higher equilibrium lattice volume and much higher total energy, it is of interest to see how the *GW* gap corrections compare in such different structures. Fig. 2 shows the crystal structures for cubic, tetragonal and orthorhombic from left to right respectively. Table II summaries the structural parameters used in the calculations, such as the lattice constants and Wyckoff positions. The relaxed lattice constant for the cubic phase in LDA is 3.86 Å which is only 1 % underestimated relative to the experiment.

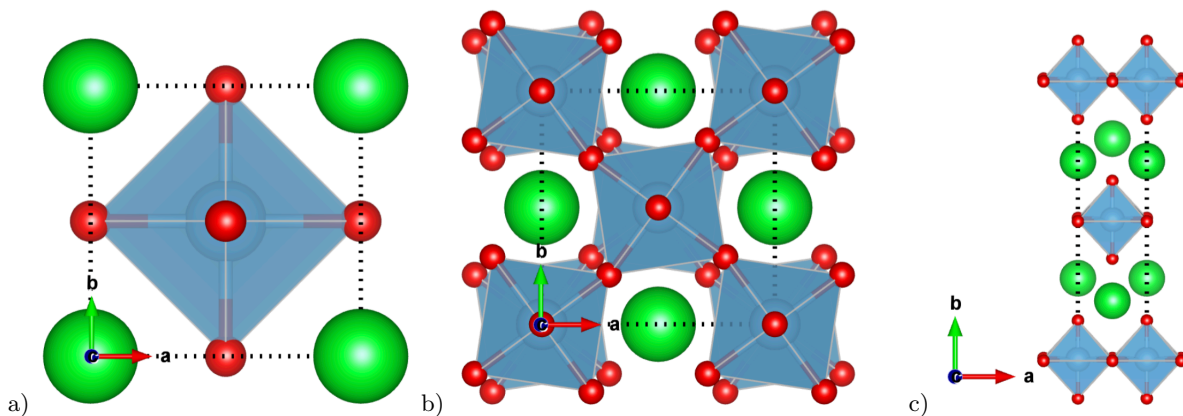


FIG. 2. Crystal structures of SrTiO₃ a) cubic, b) tetragonal $I4/mcm$, and c) layered orthorhombic CaIrO₃ view from the z -axis.

VI. RESULTS

A. Cubic STO

In Fig. 3a we show the band structure of cubic SrTiO₃ in the full QSGW approach compared with LDA. A few states at Γ are symmetry labeled for later reference. In Table III we summarize the gaps and various other band structure parameters in different approximations. In Table V we show how the different approximations affect other band states relative to the VBM. This allows us to assess to what extent the GW correction can be approximated by a \mathbf{k} and state independent scissor shift.

First, we see that our LDA gap agrees quite well with other LDA (or GGA) calculations. Second we see that the G_0W_0 gap is significantly lower than the QSGW gap. Third, unlike the pseudopotential calculations reviewed in Sec. II, the QSGW gap significantly overestimates the gap. Even if we use the 0.8Σ approach, they are still larger than experiment. It is only when we add both the 0.8Σ and lattice polarization correction, that we recover the experimental values. We also note that the 0.8Σ approach actually reduces the QSGW-LDA indirect (direct) gap shifts by about a factor 0.73 (0.74). In agreement with other calculations and already correctly described in LDA, the indirect $R - \Gamma$ gap is about 0.4 eV lower than the lowest direct $\Gamma - \Gamma$ gap. The VBM between $R - M$ is very flat and in QSGW the actual VBM lies actually in between R and M and is 0.09 eV above that at R. Finally we see that the semi-core levels play a more important role in QSGW than in LDA. Neglecting them, the gap would be only 0.07 eV lower in LDA but is 0.5 eV lower in QSGW or still 0.2 eV lower in the final LST and 0.8Σ corrected case.

B. Polaron estimates

Next, we discuss the lattice polarization correction to the gap in detail. The zero-point motion correction con-

tains a contribution from the long-range Fröhlich type of electron phonon coupling. The latter is arguably the largest electron-phonon coupling correction for a strongly ionic material with large LO-TO splitting because the other electron-phonon coupling effects tend to be smaller than 0.1 eV except for systems with all light atoms. To estimate it we follow the approach of Nery and Allen.³⁵ The main point is that the Fröhlich electron-phonon coupling behaves as $1/q$ and hence near band edges where the band difference $E_n(\mathbf{k} + \mathbf{q}) - E_n(\mathbf{k})$, which enters the denominator in the Allen-Heine-Cardona expression for the electron-phonon self-energy, gives a divergent contribution. Nery and Allen showed how it can be integrated analytically when a simple effective mass approximation is used for the bands. The length scale for the polaron effect is $a_P = \sqrt{\hbar/2m_*\omega_L}$ and if we assume we need to integrate the singular behavior only over a region in \mathbf{q} -space of size $1/a_P$ as upper limit, then the polaron shift of a band is given by²⁰

$$\begin{aligned} \Delta E_n(\mathbf{k}) &= -\alpha_P \hbar \omega_L / 2 \\ &= -\frac{e^2}{4a_P} \left(\frac{1}{\epsilon_\infty} - \frac{1}{\epsilon_0} \right), \\ &= -\frac{e^2}{4a_P \epsilon_\infty} \left(1 - \frac{\omega_T^2}{\omega_L^2} \right). \end{aligned} \quad (4)$$

In other words it essentially the change in the Coulomb interaction calculated at the polaron length scale due to the change in screening from only electronic screening to electron plus lattice screening. The extra factor 2 arises from the choice of cut-off in \mathbf{q} -space and we have written the change in macroscopic inverse dielectric constants using the Lyddane-Sachs-Teller relation. In this way, for a given LO-TO phonon pair, we have a separate contribution from each phonon, since both a_P and the dielectric constant factor depend on the phonon considered. We can thus estimate the effect for each phonon and add them, thereby generalizing Nery and Allen's simple model to the case of multiple phonons. In SrTiO₃, there are three optically active phonons.

TABLE III. Band gap in eV of cubic SrTiO₃. Here no semi-core means Sr-4*p* and Ti-3*p* semi-core states are not included.

basis-sets	k point	LDA	G_0W_0	QSGW	0.8 Σ -QSGW	QSGW+LP	QSGW+LP+0.8 Σ	Expt.
with Sr _{4<i>p</i>} ,Ti _{3<i>p</i>}	$\Gamma - \Gamma$	2.15,2.24 ^a ,2.21 ^b	4.1	4.83,3.76 ^b 5.42 ^c	4.14	4.28	3.7	3.75 ^d
no semi-core		2.08	3.85	4.31	3.8	3.83	3.5	
with Sr _{4<i>p</i>} ,Ti _{3<i>p</i>}	$R - \Gamma$	1.74	3.65	4.34,5.07 ^c ,3.32 ^d	3.64	3.78	3.2	3.25 ^e ,3.2 ^f
no semi-core ^g		1.65	3.37	3.82	3.3	3.35	3	
with Sr _{4<i>p</i>} ,Ti _{3<i>p</i>}	Γ -VBM	1.74	3.52	4.25	3.52	3.69	3.15	

^a First principle calculation by Cai Meng-Qui *et al.*^{30,31}

^b Sponza *et al.*⁵

^c Cappellini *et al.*⁷

^d Hamann and Vanderbilt⁶

^e Fundamental gap in the valence electron-loss spectroscopy^{32,33}

^f Fundamental absorption edge in reflectivity measurement of SrTiO₃³⁴

^g Without local orbital VBM is at *R*

TABLE IV. Polaron band shift estimates. The estimate in each row corresponds to a given LO-TO phonon pair. The final row gives the sum of them. The masses are in units of free electron mass, the phonon frequencies in cm⁻¹, the polaron lengths in Bohr, the band shifts in meV.

m_{le}	m_{he}	m_e	m_{hh}	m_{lh}	m_h	ω_L	ω_T	a_{Pe}	a_{Ph}	ϵ_∞	ΔE_c	ΔE_v	ΔE_g
0.33	2.65	1.10	5.08	0.67	2.14	795	547	11.19	8.03	5.52	58	81	134
0.33	2.65	1.10	5.08	0.67	2.14	474	170	14.49	10.40	5.52	74	103	177
0.33	2.65	1.10	5.08	0.67	2.14	171	91	24.12	17.32	5.52	37	51	88
Total											169	235	404

The second point is that this predicts a correction near each band edge. The conduction band at Γ and the VBM at *R* are both three-fold degenerate and anisotropic, so to apply the theory in its simple form, we need to average the effective masses in some way to extract the polaron length scale. At both points we could exploit the cubic symmetry to write a Kohn-Luttinger type of effective Hamiltonian. In our previous work²⁰ for simple di-atomic cubic compounds, we just used an average of the heavy and light masses in the cubic direction, according to the corresponding band's degeneracy. Following the same approach here, the band structure shows that it would be appropriate to use $m_h = (m_{hh} + 2m_{lh})/3$ for holes and the same for the electrons, $m_e = (m_{he} + 2m_{le})/3$ where we use the masses in the $\Gamma - X$ and $R - M$ directions, which are both simple cubic *x* directions. Thus, we obtain separate electron and hole polaron length scales a_{Pe} and a_{Ph} . Since the latter only provide estimates of the **q**-space integration region, it is not too crucial how we perform the average, although we recognize this is at present a limitation of the approach. The VBM at *R* can be seen to be rather flat and in fact in *GW* the maximum moves away from *R* toward *M*. We use the masses extracted from our QSGW bands without the lattice polarization correction. The hole polaron length scale is significantly shorter than for the electrons, predicting stronger polaronic effects for holes. This agrees with the finding in other work of self-trapped hole-polarons.^{36,37}

The results of this approach and the corresponding parameters are summarized in Table IV. We can see that the conduction band is predicted to shift less than the valence band as expected and the total gap correction is predicted to be 404 meV, which we really should round off to 0.4 eV. The shortest polaron length scale corresponds to holes for the largest phonon frequency and is 8 Bohr. This corresponds to a *q*-space region of about 1/6 of the Brillouin zone. Our estimate using the BM approach in Table III used a $4 \times 4 \times 4$ mesh and gives a contribution to the zero-point motion or lattice polarization correction of -0.55 eV. This is already rather close to the polaron estimate. With a $6 \times 6 \times 6$ mesh we obtain -0.25 eV. These bracket the polaron estimate of Table IV. We can thus conservatively conclude that the lattice polarization correction amounts to 0.3 ± 0.1 eV in good agreement between the Nery-Allen like estimate (0.4) and the BM approach. When we add this to the 0.8 Σ result we obtain a gap of 3.24 eV for the indirect gap in excellent agreement with experiment. We note that if we apply the lattice polarization correction using the BM approach with a $4 \times 4 \times 4$ mesh but then apply the 0.8 Σ correction, the LPC shift is also reduced by 0.8, and becomes 0.4 eV. We can see that in this approach the correction is almost a constant shift and hence the indirect gap correction is the same as the direct gap correction. Because of the approximate nature of these estimates, we have not separately evaluated the polaron

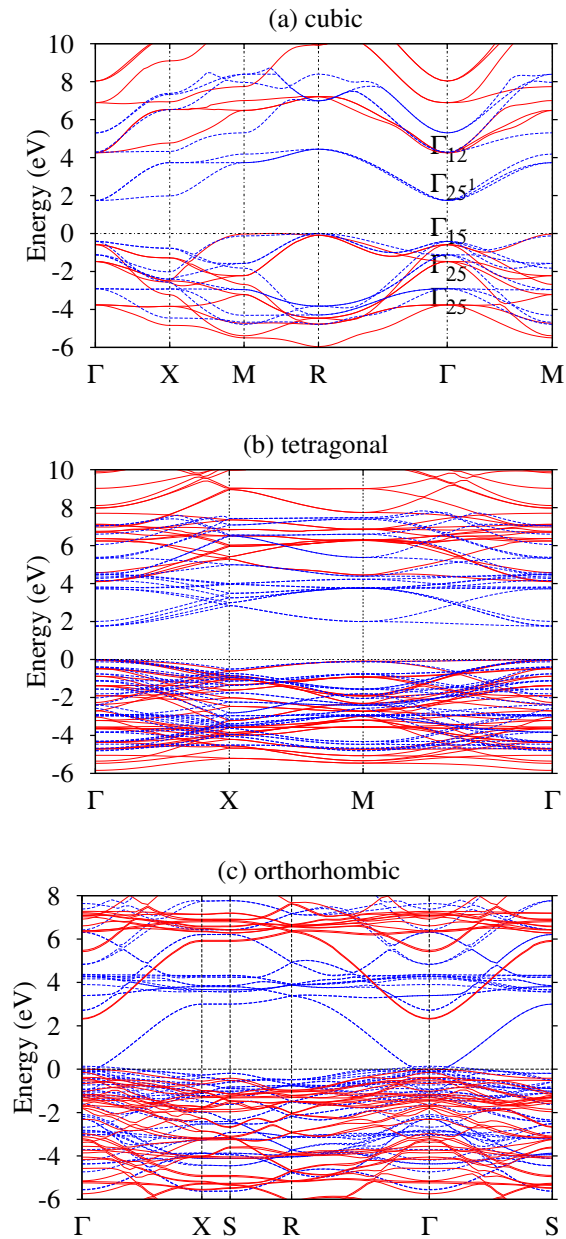


FIG. 3. (Color-online) Band structure of a) cubic and b) tetragonal SrTiO₃ c) layered orthorhombic, LDA: blue dashed and QSGW: red solid lines.

approach to the VBM at Γ which would give the direct gap. In principle, the polaronic effect also should enhance the band mass by a factor $(1 + \alpha_P/6)$ but it is not clear that the BM-method captures this more subtle effect. In fact, we find the bands to shift almost rigidly as can be seen in Fig. 4.

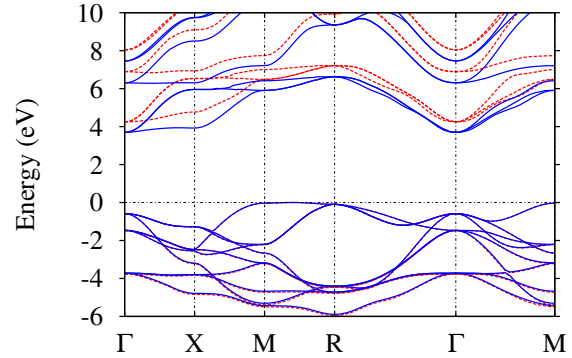


FIG. 4. Comparison of the band structure of SrTiO₃ in QSGW (red dashed) and in QSGW with lattice polarization correction using BM-approach with $4 \times 4 \times 4$ mesh (blue solid).

C. Other band structure features

Turning to other band features than the gap, summarized in Table V we see that Sr-4*p* states lie significantly closer to the VBM than the Ti 3*p* semicore states and hence play a more important role. We can see that the shifts of these states are also sensitive to the 0.8Σ and LPC corrections and amount to about 2 eV for Sr-4*p* and 4 eV for Ti 3*p*. As expected, the farther away from the VBM, the larger is the quasiparticle self-energy shift. In the conduction band we see that the higher lying Γ_{12} state has almost the same shift from LDA (about 1.4 eV) as the $\Gamma_{25'}$ CBM. In the valence band the shifts are smaller and progressively larger as we go deeper in the VBM.

D. Tetragonal structure

The band structure for the tetragonal structure is shown in Fig. 3b. In the tetragonal material we see a similar large shift of the band gap by *GW*. To understand this band structure, we note that the tetragonal unit cell is rotated by 45° and has $a_t = \sqrt{2}a_c$ as in-plane lattice constant. Thus the Brillouin zone (BZ) of the cubic structure is folded into a smaller BZ with the $\Gamma - M$ of the tetragonal BZ corresponding to half the $\Gamma - X$ of the cubic BZ. The high symmetry points correspond to $M = (1/2, 1/2, 0)$ and $X = (1/2, 0, 0)$ with respect to their respective reciprocal lattice vectors. Similarly the $\Gamma - X$ of the tetragonal BZ is half the $\Gamma - M$ of the cubic BZ. One can clearly see the folding in half of the bands with additional small gaps opening due to the breaking of the symmetry by the slight rotation of the octahedra. We can see that VBM which in the cubic case and in QSGW occurs between $M - R$ ($R = (1/2, 1/2, 1/2)$), where the band dispersion is very flat, is folded on to the tetragonal

TABLE V. Various band differences: specific states (symmetry labeling as in Fig. 3a) in the conduction band relative to the CBM, and in the upper valence band relative to the VBM. The position of the semicore states Sr_{4p} , Ti_{3p} , are also with respect to the VBM at R .

	$\Gamma_{25'}$ -CBM	Γ_{12} -CBM	Γ_{15} -VBM	Γ_{25} -VBM	Γ_{25} -VBM	Sr_{4p} states	Ti_{3p} states
LDA	1.74	4.29	-0.41	-1.12	-2.91	-14.66	-32.55
G_0W_0	3.53	6.29	-0.58	-1.37	-3.49	-17.19	-36.48
QSGW	4.34	6.98	-0.49	-1.39	-3.67	-17.51	-37.38
0.8 Σ -QSGW	3.54	6.17	-0.49	-1.32	-3.64	-16.9	-36.74
QSGW+LP	3.78	6.4	-0.49	-1.37	-3.62	-17.51	-37
QSGW+LP+0.8 Σ	3.2	5.71	-0.49	-1.31	-3.5	-16.9	-36.4

TABLE VI. Band gap of tetragonal $SrTiO_3$ in eV at $\Gamma - \Gamma$.

basis-sets	LDA	QSGW	QSGW +LPC	QSGW 0.8 Σ +LPC	Ref.
with Sr_{4p}, Ti_{3p}	1.76	4.1	3.88	3.27	4.03 ^a
no semi-core	1.72	3.7	3.47	3.04	

^{a, b} By Heifets and *et al.*³⁸ using a hybrid DFT-Hartree-Fock (HF) approach

BZ Γ point and the gap becomes direct.

E. Hypothetical layered orthorhombic structure

Although, the $CaIrO_3$ structure, proposed²⁶ for $SrTiO_3$ as a potential high-pressure structure, can be shown to be unstable,²⁷ it is of interest to see how the GW gap correction changes with such a large change in structure. This structure has edge-sharing octahedra in layers separated by Sr, rather than corner sharing octahedra. In the LDA, the band gap becomes zero as can be seen in Fig. 3c. The very different band dispersion in this case results from the direct Ti-d to Ti-d interactions between much closer Ti atoms in the layer. In the QSGW method the gap becomes 2.32 eV which is not too different from the gap correction 2.68 eV in cubic perovskite. The gap correction is found to be almost the same as in the cubic or tetragonal structures. Similar screening reduction or 0.8 Σ corrections and lattice polarization corrections should apply here but are not further pursued at this point.

VII. CONCLUSIONS

In this paper we reviewed the status of the QSGW method for a prototypical complex transition metal oxide like $SrTiO_3$ in the perovskite structure. We found that all-electron QSGW results obtained by means of the FP-LMTO implementation give a significant overestimate of the gap compared to experiment in contrast to PAW or pseudopotential based GW approaches. This

indicates a compensation of errors in the latter. We base this on the observation that for a large family of materials, the under-screening of W in the RPA amounts to about 20 % and can hence be accommodated by using the 0.8 Σ approach. This evidence is based both on the comparison of dielectric constants in QSGW with experiment and on recent calculations^{11,13} which go beyond the RPA by including an exchange correlation kernel in the calculation of W or adding vertex corrections directly¹² and it is found to apply to both tetrahedrally bonded semiconductors and various oxides and ionic compounds. The second important correction to the gap is the lattice polarization correction. This is part of the zero-point motion correction due to electron-phonon coupling and more specifically is its dominant contribution in strongly ionic materials arising from the long-range Fröhlich part of the electron-phonon coupling. Two independent estimates of this effect were made: one based on the polaron theory and one on the Botti-Marques approach of multiplying the macroscopic dielectric constant at $\mathbf{q} = 0$ by a Lyddane-Sachs-Teller factor along with a suitable \mathbf{q} -mesh sampling based itself on the polaron length scale which determines the strength of the effect. The two estimates are found to be in good agreement with each other. We find that both the electron-hole interaction effects which reduce Σ by about 20 % and the lattice-polarization corrections are required to obtain good agreement with experimental gaps in cubic perovskite $SrTiO_3$. As for the structural dependence of the QSGW corrections, we find that the gap correction in tetragonal STO is very close to that in cubic STO and the bands are essentially folded according to the rotation of the octahedra, which leads to a doubling of the cell and rotation of the BZ by 45°. This happens to fold the R point of the BZ onto the Γ -point and hence the indirect lowest gap becomes then direct. Due to the similarity in band states, we expect it to be pseudo-direct in the sense that no strongly optical transitions will correspond to this direct gap. Even for a very different hypothetical structure with edge-sharing octahedra, we find very similar gap corrections by QSGW, which shows that the gap corrections are rather insensitive to structure.

ACKNOWLEDGMENTS

This work was supported by the US Department of Energy, Office of Science, Basic Energy Sciences under grant

No. DE-SC0008933. Calculations made use of the High Performance Computing Resource in the Core Facility for Advanced Research Computing at Case Western Reserve University. MvS was supported by EPSRC CCP9 Flagship Project No. EP/M011631/1.

-
- ¹ M. Methfessel, M. van Schilfgaarde, and R. A. Casali, in *Electronic Structure and Physical Properties of Solids. The Use of the LMTO Method*, Lecture Notes in Physics, Vol. 535, edited by H. Dreyssé (Berlin Springer Verlag, 2000) p. 114.
- ² T. Kotani and M. van Schilfgaarde, *Phys. Rev. B* **81**, 125117 (2010).
- ³ M. van Schilfgaarde, T. Kotani, and S. Faleev, *Phys. Rev. Lett.* **96**, 226402 (2006).
- ⁴ T. Kotani, M. van Schilfgaarde, and S. V. Faleev, *Phys. Rev. B* **76**, 165106 (2007).
- ⁵ L. Sponza, V. Véniard, F. Sottile, C. Giorgetti, and L. Reining, *Phys. Rev. B* **87**, 235102 (2013).
- ⁶ D. R. Hamann and D. Vanderbilt, *Phys. Rev. B* **79**, 045109 (2009).
- ⁷ G. Cappellini, S. Bouette-Russo, B. Amadon, C. Noguera, and F. Finocchi, *Journal of Physics: Condensed Matter* **12**, 3671 (2000).
- ⁸ T. Kotani, M. van Schilfgaarde, S. V. Faleev, and A. Chantis, *Journal of Physics: Condensed Matter* **19**, 365236 (2007).
- ⁹ D. Deguchi, K. Sato, H. Kino, and T. Kotani, *Jap. J. Appl. Phys.* **55**, 051201 (2016).
- ¹⁰ S. Ismail-Beigi, *Journal of Physics: Condensed Matter* **29**, 385501 (2017).
- ¹¹ W. Chen and A. Pasquarello, *Phys. Rev. B* **92**, 041115 (2015).
- ¹² A. L. Kutepov, *Phys. Rev. B* **95**, 195120 (2017).
- ¹³ M. Shishkin, M. Marsman, and G. Kresse, *Phys. Rev. Lett.* **99**, 246403 (2007).
- ¹⁴ A. N. Chantis, M. van Schilfgaarde, and T. Kotani, *Phys. Rev. Lett.* **96**, 086405 (2006).
- ¹⁵ A. N. Chantis, M. Cardona, N. E. Christensen, D. L. Smith, M. van Schilfgaarde, T. Kotani, A. Svane, and R. C. Albers, *Phys. Rev. B* **78**, 075208 (2008).
- ¹⁶ S. Rigamonti, S. Botti, V. Veniard, C. Draxl, L. Reining, and F. Sottile, *Phys. Rev. Lett.* **114**, 146402 (2015).
- ¹⁷ A. L. Kutepov, *Phys. Rev. B* **94**, 155101 (2016).
- ¹⁸ L. Hedin, *Phys. Rev.* **139**, A796 (1965).
- ¹⁹ L. Hedin and S. Lundqvist, in *Solid State Physics, Advanced in Research and Applications*, Vol. 23, edited by F. Seitz, D. Turnbull, and H. Ehrenreich (Academic Press, New York, 1969) pp. 1–181.
- ²⁰ W. R. L. Lambrecht, C. Bhandari, and M. van Schilfgaarde, *Phys. Rev. Materials* **1**, 043802 (2017).
- ²¹ S. Botti and M. A. L. Marques, *Phys. Rev. Lett.* **110**, 226404 (2013).
- ²² C. Friedrich, S. Blügel, and A. Schindlmayr, *Phys. Rev. B* **81**, 125102 (2010).
- ²³ T. Kotani, *Journal of the Physical Society of Japan* **83**, 094711 (2014), <http://dx.doi.org/10.7566/JPSJ.83.094711>.
- ²⁴ <https://www.questaal.org/>, Our *GW* implementation was adapted from the original ecalj package now at <https://github.com/tkotani/ecalj/>.
- ²⁵ E. Bott, M. Methfessel, W. Krabs, and P. C. Schmidt, *Journal of Mathematical Physics* **39**, 3393 (1998).
- ²⁶ D. Cabaret, B. Couzinet, A. Flank, J. Iti, P. Lagarde, and A. Polian, *AIP Conference Proceedings* **882**, 120 (2007).
- ²⁷ C. Bhandari and W. R. L. Lambrecht, “Instability of the layered orthorhombic post-perovskite phase of SrTiO₃,” (2017), unpublished.
- ²⁸ Y. A. Abramov, V. G. Tsirelson, V. E. Zavodnik, S. A. Ivanov, and B. I. D., *Acta Crystallographica Section B* **51**, 942 (1995).
- ²⁹ W. Jauch and A. Palmer, *Phys. Rev. B* **60**, 2961 (1999).
- ³⁰ M.-Q. Cai, Z. Yin, and M.-S. Zhang, *Chemical Physics Letters* **388**, 223 (2004).
- ³¹ G. Gupta, T. Nautiyal, and S. Auluck, *Phys. Rev. B* **69**, 052101 (2004).
- ³² K. van Benthem, C. Elssser, and R. H. French, *J. Appl. Phys.* **90**, 6156 (2001).
- ³³ D. Buerle, W. Braun, V. Saile, G. Sprssel, and E. Koch, *Zeitschrift für Physik B Condensed Matter* **29**, 179 (1978).
- ³⁴ M. Cardona, *Phys. Rev.* **140**, A651 (1965).
- ³⁵ J. P. Nery and P. B. Allen, *Phys. Rev. B* **94**, 115135 (2016).
- ³⁶ A. Janotti, J. B. Varley, M. Choi, and C. G. Van de Walle, *Phys. Rev. B* **90**, 085202 (2014).
- ³⁷ P. Erhart, A. Klein, D. Åberg, and B. Sadigh, *Phys. Rev. B* **90**, 035204 (2014).
- ³⁸ E. Heifets, E. Kotomin, and V. A. Trepakov, *Journal of Physics: Condensed Matter* **18**, 4845 (2006).